Russian Geology and Geophysics © 2024, Novosibirsk State University
Available online in February, pp. 1–16, 2024 *DOI:10.2113/RGG20234637* *Geologiya i Geofizika*

Active Tectonic Deformation of the Qilian Shan, Northeastern Tibetan Plateau

Zhidan Chen[a,b,✉], N.V. Koronovskii[a], V.A. Zaitsev[a], Wenbin Xu[b], E.A. Manuilova[a,c], Xiaoge Liu[b]

[a]*Lomonosov Moscow State University, Leninskie Gory 1, Moscow, 119991, Russia*

[b]*School of Geosciences and Info-Physics, Central South University, 932 Lushan South Road, Changsha, 410083, China*

[c]*Schmidt Institute of Physics of the Earth, Russian Academy of Sciences, ul. Bol'shaya Gruzinskaya 10, bld. 1, Moscow, 123242, Russia*

Received 5 June 2023; accepted 25 October 2023

Abstract—The Qilian Shan (or Qilian Mountains), located on the northeastern margin of the Tibetan Plateau, is an actively growing orogenic belt resulting from the far-field impact of the India–Eurasia collision. The northward penetration of the Indian Plate is responsible for intense crustal shortening in the Qilian Shan. However, the tectonic deformation pattern in response to the crustal shortening remains unclear. In this study, we present the regional seismicity, fault activity, and GPS crustal movement velocity field to characterize the active tectonic deformation of the Qilian Shan based on historical data over the past two decades. The results suggest that the western Qilian Shan is characterized by distributed north–south crustal shortening, while the eastern Qilian Shan is dominated by blocklike eastward extrusion of crust along major strike-slip faults coupled with clockwise rotation. North–south crustal shortening and east–west lateral extrusion, two deformation modes responding to the India–Eurasia convergence, match the crustal deformation in the Qilian Shan. The tectonic deformation of the western Qilian Shan is largely in agreement with the former, while the eastern Qilian Shan corresponds closely to the latter. Lower crustal flow beneath the central Tibetan Plateau provides the potential driving force to induce the eastward extrusion of crustal material out of the plateau and the growth of some boundary mountain ranges, such as the Qilian Shan.

Keywords: active tectonic deformation; seismicity; fault activity; GPS velocity field; Qilian Shan; Tibetan Plateau

INTRODUCTION

The orogeny and tectonic deformation of the Tibetan Plateau resulting from the India–Eurasia collision are among the most important geologic events occurring in the Cenozoic on the Earth (Molnar and Tapponnier, 1975; Yin and Harrison, 2000; Royden et al., 2008). The ongoing northward penetration of the Indian Plate leads to considerable crustal shortening in Tibet, Pamir, the Tien Shan ("Shan" means "mountain" in Chinese), and other mountain ranges in Central Asia (Fig. 1*A*) (Burtman, 2012). The GPS measurements indicate that the present-day rate of the convergence between India and Eurasia is 40–50 mm/yr, but only 18 ± 2 mm/yr is absorbed by the Himalayan thrust system. The remaining 20–30 mm/yr is transferred to tectonic deformation in mountain ranges farther north (Wang et al., 2001; Zhang et al., 2004). GPS velocity profiles across the Tibetan Plateau in the northeastern direction, parallel to the direction of the India–Eurasia collision, indicate a general linear decreasing trend of the velocity gradient (Wang et al., 2001). The titanic thrust structures in south Tibet and the widely distributed fold-and-thrust belts on the northeastern margin of the Tibetan Plateau are considered to be the main deformation modes to accommodate crustal shortening (Molnar and Tapponnier, 1975; Zhang et al., 2004; Chen et al., 2022). Several large-scale strike-slip faults and extensional structures in the central Tibetan Plateau indicate that significant strike-slip deformation and east–west extension occur in the interior of the plateau, and the causes of these structures and their roles in accommodating strain distribution within the plateau remain unclear (Fig. 1*A*) (Molnar and Tapponnier, 1975; Tapponnier et al., 1981; Yin and Harrison, 2000; Zhang et al., 2004). The discoveries of the strike-slip and extensional structures inspire vigorous debate about the deformation patterns and mechanisms in response to the India–Eurasia collision and, meanwhile, profoundly influence our understanding of the geodynamics of intracontinental deformation.

Two geodynamic models have been proposed to characterize the tectonic deformation of the Tibetan Plateau in response to crustal shortening due to the India–Eurasia collision (Zhang et al., 2004). The "crustal thickening model" assumes that the crustal shortening is absorbed by the continuous thickening and compression deformation within blocks and at the boundaries, while the "crustal extrusion model" suggests that the crustal shortening is largely compensated for by the lateral movement of the blocks in the latitudinal direction along the boundary strike-slip faults (Zhang et al., 2004; Liu et al., 2022). The former applies to tectonic deformation at the southern and northern margins

✉ Corresponding author.
E-mail address: chenzhidan188@163.com (Zhidan Chen)

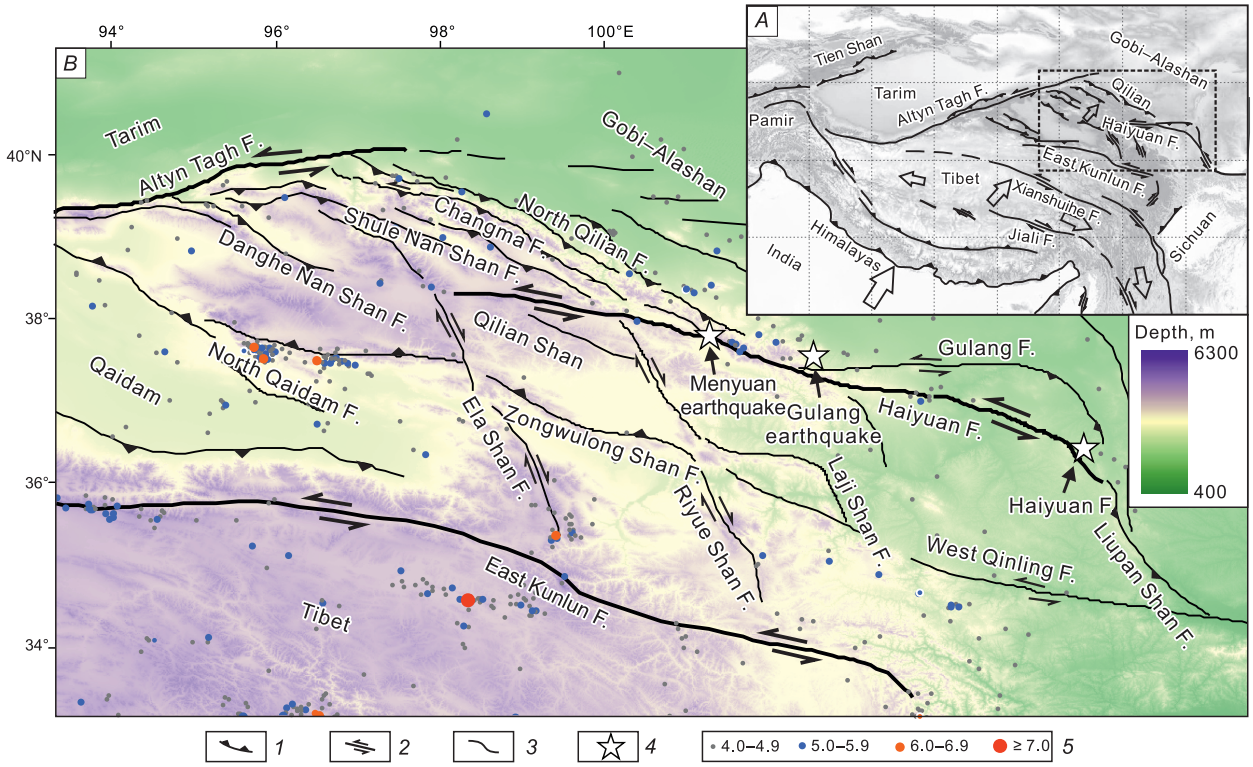

Fig. 1. Tectonic setting map of the Qilian Shan, northeastern Tibetan Plateau. *A* – Tectonic configuration of the Tibetan Plateau; *B* – topographic map of the Qilian Shan and its surrounding areas showing the main active faults and historical earthquakes, *1* – reverse fault, *2* – strike-slip fault, *3* – other fault, *4* – large earthquakes, *5* – historical earthquakes. The historical earthquake data are downloaded from the China Earthquake Networks Center (CENC: www.ceic.ac.cn/history) and the Global Centroid Moment Tensor (GCMT: www.globalcmt.org). The range of the map is shown in the black dashed rectangle of panel *A*. F. – Fault.

of the Tibetan Plateau, the Himalayan and Qilian mountain ranges (Yin and Harrison, 2000; Zhang et al., 2004). The latter is supported by evidence from the central plateau, where several large-scale subparallel strike-slip faults (e.g., Jiali, Xianshuihe, and East Kunlun faults) and a series of normal faults due to E–W extension are considered to be the results of the eastward extrusion of crustal materials (Tapponnier et al., 1981). Both models can reveal part of the tectonic phenomenon occurring in Tibet, but neither is able to comprehensively depict the deformation features of the Tibetan Plateau. More recently, some have suggested that the active blocks that make up the Tibetan Plateau may have different deformation modes because of the spatial heterogeneity of rock strength and lithospheric rheology (Wang et al., 2003; Wang and Shen, 2020; Li et al., 2021).

The Qilian Shan, located on the northeastern margin of the Tibetan Plateau, is an actively growing orogenic belt formed during the northward expansion of the plateau and, therefore, appears to be the latest component of the Tibetan Plateau (Fig. 1*B*). Recent studies show that the Qilian Shan began to uplift in the middle Miocene (14–10 Ma) (Wang et al., 2017; Zheng et al., 2017a), much later than the onset of the India–Asia collision (60–40 Ma) (Yin and Harrison, 2000; Royden et al., 2008). Despite its later formation, strong crustal shortening caused mountain ranges to rise over 3000 km relative to the neighboring Gobi–Alashan basin (Fig. 1*B*). The wide distribution of a series of WNW-trending mountain ranges and thrust faults indicates that the Qilian Shan appears to be dominated by north–south crustal shortening (Fig. 1*B*) (Wang et al., 2001; Zhang et al., 2004). However, other finds in regard to many large-scale strike-slip faults and shear-type earthquakes show that there is intense shear deformation besides compression (Zhang et al., 2007; Zheng et al., 2013). Seismic data and their focal mechanisms suggest that this region hosts not only a large number of compressional earthquakes but also a wide distribution of strike-slip events (Meng et al., 2022), indicating strong seismicity and tectonic complexity in the Qilian Shan. Paleoseismic investigations show that several damaging earthquakes, including the 1920 Haiyuan $M \approx 8.5$ earthquake and the 1927 Gulang $M \approx 8.0$ earthquake, occurred in this region (Fig. 1*B*). The Haiyuan earthquake is a left-lateral event, and the Gulang earthquake is compressional (Liu-Zeng et al., 2007). Recently, on 8 January 2022, the $M_s = 6.9$ Menyuan earthquake with left-lateral strike-slip occurred in the middle part of the Haiyuan fault (Fig. 1*B*) (Feng et al., 2022; Yang et al., 2022). Diverse seismic events and fault activities indicate the complexity of crustal deformation in the Qilian Shan. However, it is unclear how the Qilian Shan accommodates crustal shortening and which geodynamic models are compatible with the tectonic deformation in the Qilian Shan.

In this study, we collected seismic sequences, GPS data, and published results on active faults in the Qilian Shan over the past two decades. Then, we analyzed and summarized the regional seismicity, kinematics of the main active faults, and GPS crustal movement velocity field to characterize the active tectonic deformation and deformation pattern of the Qilian Shan, which is of great significance for shedding light on the deformation modes and geodynamics of intracontinental orogenic belts and assessing regional seismic risks.

TECTONIC SETTING OF THE STUDY AREA

The Qilian Shan is confined by the Altyn Tagh fault in the west, by the Haiyuan–Liupan Shan fault in the east, and by the north Qilian and north Qaidam mountain frontal thrust systems in the north and south (Fig. 1*B*) (Hu et al., 2021). Series of band-shaped mountain ranges, compressional basins, and fold-and-thrust belts are widely distributed in the Qilian Shan along the NWW direction, roughly perpendicular to the collision orientation between the Indian and Eurasian plates, indicating that the Qilian Shan is largely dominated by north–south compression (Fig. 1*B*) (Chen et al., 2022). GPS data suggest the shortening rate of the Qilian Shan is 5–8 mm/yr (Zhang et al., 2004; Pan et al., 2020), widely dissipated by the NWW-trending mountain ranges and fold-and-thrust belts (Chen et al., 2022).

Cenozoic structures of the Qilian Shan consist of a series of NWW-directed fold-and-thrust belts and several strike-slip faults (Ding, 1984; Deng, 1996). The major strike-slip faults are the Altyn Tagh fault to the northwest, the Haiyuan fault to the northeast, and the Ela Shan and Riyue Shan faults in the interior of the Qilian Shan (Fig. 1*B*). Almost all the NWW-directed thrust faults and thrust-related folds are developed along the tectonically active mountain fronts in the Qilian Shan (Hetzel, 2013; Chen et al., 2022). The NNW-directed Ela Shan and Riyue Shan faults are right-lateral strike-slip faults with normal or reverse components within the Qilian Shan (Fig. 1*B*) (Yuan et al., 2011; Chen et al., 2021). Two continental-scale strike-slip faults, the Altyn Tagh and Haiyuan faults, constitute the northern boundary of the Tibetan Plateau and accommodate the eastward motion of the Tibetan Plateau with respect to its northern Tarim and Gobi–Alashan basins (Fig. 1*B*). The GPS data and geological results reveal that the left-lateral slip rate of the Altyn Tagh fault decreases from 10–12 mm/yr in the middle segment to 1–2 mm/yr in the easternmost section (Xu et al., 2005; Zhang et al., 2007; Zheng et al., 2013). The rate decrease occurs largely at the junction zones between the Altyn Tagh fault and NWW-trending mountain ranges of the western Qilian Shan (Liu et al., 2020; Chen et al., 2022). Contrary to the decreasing trend of the Altyn Tagh fault, the slip rate of the Haiyuan fault shows an increase from west to east. The slip rate of the Haiyuan fault is about 1–2 mm/yr in the western segment of the fault and then increases to 4–6 mm/yr in the middle segment (Zheng et al., 2013). The spatial variation of slip rates along the major strike-slip faults indicates that ~8 mm/yr of the left-lateral slip rate on the Altyn Tagh fault is absorbed by thrusting and folding within the Qilian Shan and partially transferred into the Haiyuan fault (Zheng et al., 2013; Chen et al., 2022). However, the deformation pattern of how the Qilian Shan absorbs the considerable slip rate of the Altyn Tagh fault and transfers it into the Haiyuan fault remains unclear (Chen et al., 2022).

Given the differences in regional topography and tectonic deformation, bounded by the Ela Shan and Haiyuan faults, the Qilian Shan is divided into two parts: western and eastern Qilian Shan (Fig. 2). The western Qilian Shan consists of many NWW-directed compressional mountain ranges and basins, thrust faults, and fault-related folds, while the eastern Qilian Shan is composed of fewer NWW-directed mountain ranges, thrust faults, and several strike-slip faults (Fig. 1*B*). Based on the lithology distribution and regional faulting, the Qilian Shan is further partitioned into several active blocks: the Hexi Corridor, North Qilian, Central Qilian, South Qilian, Qinghaihu, Gonghe, Xining, Tongxin, Lanzhou, and Gannan blocks (Fig. 2) (Deng, 1996; Li et al., 2018; Hu et al., 2021).

MATERIALS AND METHODS

Seismic activities are closely correlated with regional tectonic structures. Long-term seismic information recorded by seismic stations can reflect not only the activity of the seismogenic fault but also the regional tectonic deformation. Abundant seismic records enable us to exhibit the spatial variation of regional seismic activities. Focal-mechanism solutions derived by focal parameter inversion, combined with available active-fault information, can explicitly reveal the fault slip behavior and the deformation characteristics. In this study, we collected the seismic sequences with magnitudes above three in the Qilian Shan from 2009 to 2021 (Guo et al., 2022). We then plotted the focal-mechanism solutions of these earthquakes using the GMT software (Wessel et al., 2019) and projected them onto the shadow topographic map to reveal the spatial distribution of seismic activity in the Qilian Shan. The earthquake data and focal parameters are downloaded from the National Earthquake Data Center in China (data.earthquake.cn).

The kinematics of active faults is dominated by regional tectonic backgrounds. The kinematic information of faults includes fault geometry, slip behavior, slip rate, and other parameters that, in turn, can reflect the tectonic deformation and stress–strain state (Ding, 1984; Deng, 1996; Hetzel, 2013). Among them, the slip rate of a fault is a key parameter, which can reflect not only the intensity of faults but also the regional tectonic deformation and seismic hazards. In this paper, we collected information about the fault geometry, slip behaviors, and slip rates of the main active faults

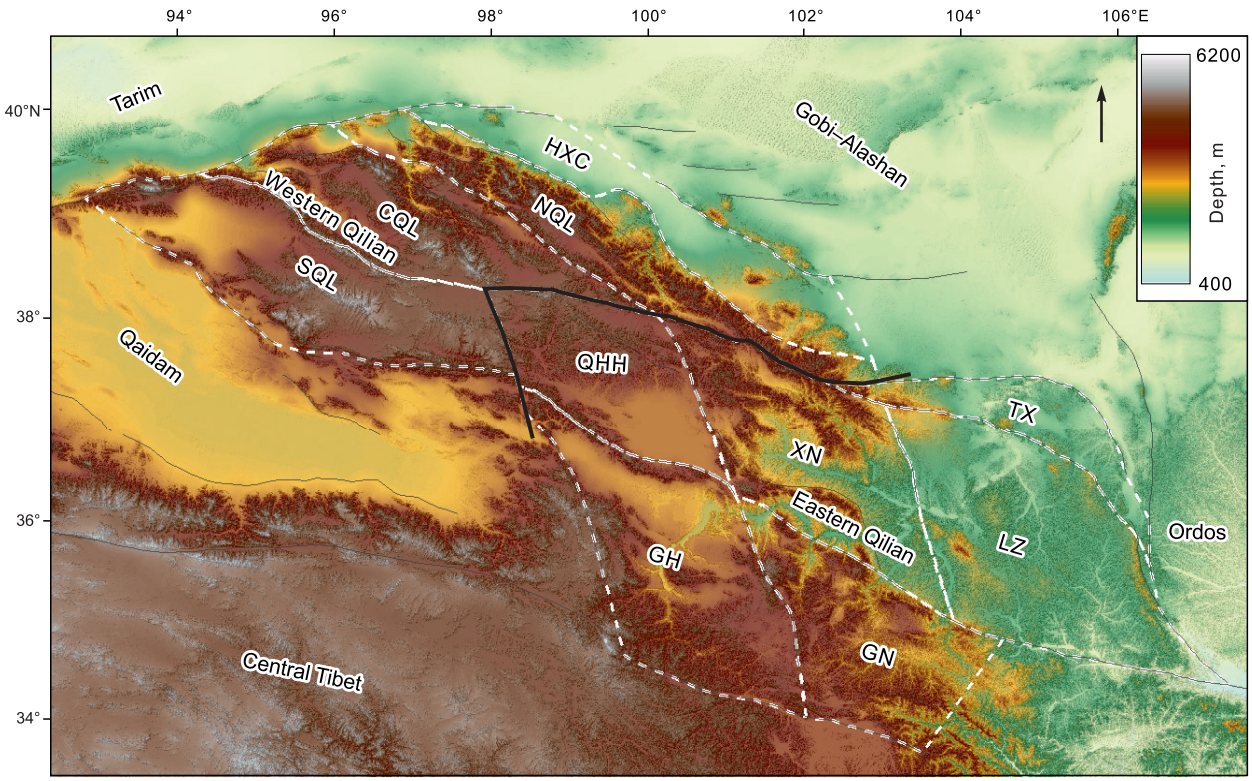

Fig. 2. Active blocks in the Qilian Shan. The white dashed lines are the boundaries of the active blocks. The thick black line marks the boundary between the western and eastern Qilian Shan. The thin gray lines are the main active faults in this region. The blocks are named as follows: HXC – Hexi Corridor block; NQL – North Qilian block; CQL – Central Qilian block; SQL – South Qilian block; QHH – Qinghaihu block; GH – Gonghe block; XN – Xining block; TX – Tongxin block; LZ – Lanzhou block; GN – Gannan block (Li et al., 2018; Hu et al., 2021).

in the Qilian Shan, which can shed light on the crustal deformation characteristics. Data on regional active faults are taken from the Seismic Active Fault Survey Data Center in China (www.activefault-datacenter.cn/map). Fault slip rates are derived from previously published studies on active faults.

The Global Positioning System (GPS), a type of space geodetic tools, provides high precision, great spatial coverage, and near real-time quantitative data on crustal movements and has been effectively applied in the crustal deformation monitoring in many active tectonic belts on the Earth (Kreemer et al., 2014). Since the 1990s, GPS crustal deformation monitoring has been carried out on the Tibetan Plateau and its neighboring regions (Wang et al., 2001; Zhang et al., 2004; Gan et al., 2007). In particular, the establishment of the Crustal Movement Observation Network of China (CMONOC) enabled large-scale monitoring of the deformation field over entire continental China (Wang and Shen, 2020). Here, we collected the GPS observation data in the Qilian Shan and its surrounding areas obtained from 1998 to 2015 from CMONOC I/II projects (Zheng et al., 2017b). Then, we processed GPS data and derived the crustal movement velocity field using the GMT software (Wessel et al., 2019). Finally, the present-day crustal strain distribution and tectonic deformation in the Qilian Shan were analyzed based on the GPS velocity field.

REGIONAL SEISMICITY

On the basis of the spatial distribution of focal-mechanism solutions derived from seismic data in the past decades, the western Qilian Shan exhibits relatively scattered distribution. Earthquakes in the western Qilian Shan are widely distributed along the NWW-trending faults within blocks, especially the Central and North Qilian blocks. In the South Qilian block, earthquakes are mainly distributed on the north Qaidam fault and its mountain frontal thrust belts (Fig. 3). In addition, the western Qilian Shan is primarily dominated by compression-type earthquakes, with limited strike-slip or tension events in the junction zones (Fig. 3). Compression-type events are generally distributed along the NWW-trending faults in the western Qilian Shan, mainly in the western segment of the North Qilian and the middle segment of the South Qilian. Tension-type events are very rare, with small magnitudes. Strike-slip events are mainly distributed on the eastern and western sides of the western Qilian Shan, at the intersections of NWW-trending thrusts and strike-slip faults on both sides (Fig. 3).

Contrary to the scattered seismic distribution in the western Qilian Shan, seismic activities in the eastern Qilian Shan are relatively concentrated, and earthquakes are largely distributed on the boundary faults, that is, the Haiyuan and Ela

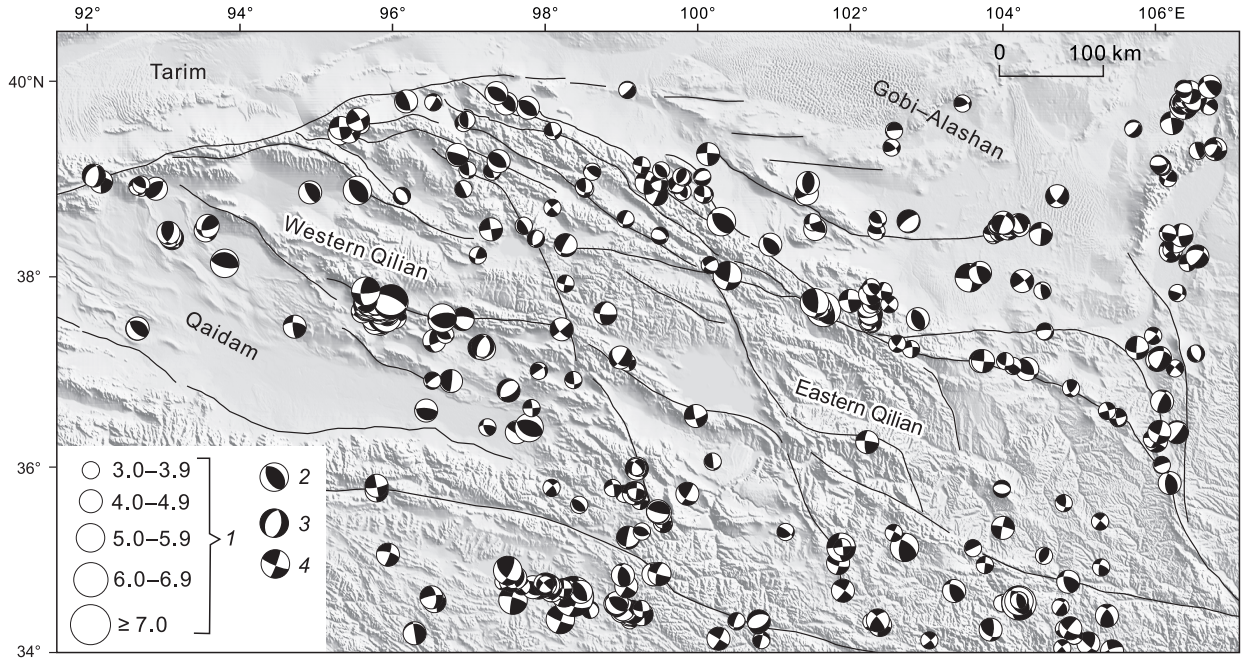

Fig. 3. Spatial distribution and focal mechanism solutions of historical earthquakes with magnitude ＞3 from 2009 to 2021 in the Qilian Shan and its surrounding areas. Black lines denote regional active faults. The earthquake data are downloaded from the National Earthquake Data Center in China (data.earthquake.cn). *1* – earthquake types, *2* – compression, *3* – tension, *4* – strike-slip.

Shan faults (Fig. 3). Except for the Gannan block with some seismic events, there is almost no notable seismic activity within blocks in the eastern Qilian Shan, such as the Qinghaihu, Gonghe, Xining, Tongxin, and Lanzhou blocks (Figs. 2, 3). Surrounded by large strike-slip faults, the eastern Qilian Shan is characterized by strike-slip type earthquakes along the boundary faults, the Haiyuan and Liupan Shan faults, with a few compression-type and tension-type events in the stepover, conjunction, and bend areas (Figs. 1*B*, 3).

To investigate the stress state of the Qilian Shan and its surrounding areas, Meng et al. (2022) conducted a horizontal projection of 877 focal-mechanism solutions in the region to determine the orientations of the *T* and *P* axes. Overall, the *P* axis exhibits a predominant orientation to the northeast, indicating that the Qilian Shan is primarily influenced by collision between the Indian and Eurasian plates. The *T* axis direction in the western Qilian Shan primarily aligns with the NE and NW, suggesting that the western Qilian Shan experiences both compressional and shear deformation, consistent with the predominant compression-type earthquakes and locally distributed strike-slip events in the region. Meanwhile, in the eastern Qilian Shan, the *P* and *T* axes demonstrate NE and NW orientations subhorizontally conjugate to each other, indicating intense shear deformation along the Haiyuan fault.

On the basis of the seismic spatial distribution and focal-mechanism solutions, it is preliminarily assumed that the western Qilian Shan is primarily characterized by scattered compression deformation with less compression and rare shear, whereas the eastern Qilian Shan is characterized by centralized shear deformation along the boundary faults of blocks with local compression and extension.

ACTIVE FAULTS AND THEIR SLIP RATES

Two continental-scale left-lateral strike-slip faults, the Altyn Tagh and Haiyuan faults, determine the northeastern and northwestern boundaries of the Qilian Shan. The interior of the Qilian Shan is characterized by several NWW-trending mountain ranges and thrust faults (Zheng et al., 2017a). Besides, two large NNW-trending dextral strike-slip faults, the Ela Shan and Riyue Shan faults, accommodate the relative displacements between blocks (Fig. 4). In this part, we summarized previously published results on major active faults and derived the late Quaternary slip rates of faults estimated by the deformed geomorphologic markers and the present-day slip rates from GPS measurements.

The Altyn Tagh and Haiyuan faults

The left-lateral Altyn Tagh fault defines the northern boundary of the Tibetan Plateau, extending for up to 1600 km between ~80 °E and ~98 °E. Early studies estimated the late Quaternary slip rate on the main slip section of the Altyn Tagh fault to be 20–30 mm/yr by dating the displaced alluvial fans and river terraces (Peltzer et al., 1989; Mériaux et al., 2004, 2005). However, these rates were much higher than the contemporary slip rates of ~10 mm/yr suggested by GPS measurements (Shen et al.,

Table 1. Slip rates of main active faults in the Qilian Shan

Faults	Segments	Slip rates (mm/yr)	References
Altyn Tagh	Western	17.5 ± 2 (left-lateral)	Xu et al., 2005
	Middle	8–12 (left-lateral)	Xu et al., 2005; Zhang et al., 2007; Cowgill, 2007
	Mideastern	4–5 (left-lateral)	Xu et al., 2005; Liu et al., 2020
	Eastern	1–2 (left-lateral)	Xu et al., 2005; Zhang et al., 2007
Haiyuan	Western	1–2 (left-lateral)	Zheng et al., 2013; Huang et al., 2022
	Middle	4–6 (left-lateral)	Zheng et al., 2013; Yao et al., 2019; Liu et al., 2022; Huang et al., 2022
	Eastern	1–2 (left-lateral)	Zheng et al., 2013; Liu et al., 2022; Huang et al., 2022
North Qilian	Western	0.4–0.8 (shortening)	Hetzel, 2013; Chen et al., 2022
	Middle	0.8–1.2 (shortening)	Hetzel, 2013; Yang et al., 2018
	Eastern	0.6–0.8 (shortening)	Hu et al., 2015
Changma	Western	0.3–0.7 (vertical); 1.4–3.7 (left-lateral)	Luo et al., 2013; Du et al., 2019
Shule Nan Shan	Eastern	0.9 ± 0.1 (vertical); 1.5 ± 0.1 (shortening)	Hu et al., 2021
Danghe Nan Shan	Western	4–5 (left-lateral)	Liu et al., 2020
	Middle	0.6 ± 0.2 (vertical) 0.8 ± 0.2 (shortening)	Xu et al., 2021
North Qaidam	Eastern	0.5–0.8 (shortening)	Shao et al., 2019; Zhang et al., 2022
Ela Shan	Middle	1.1–2.6 (right-lateral)	Yuan et al., 2011; Chen et al., 2021; Li et al., 2018
Riyue Shan	Northern	1.2 ± 0.4 (right-lateral)	Yuan et al., 2011; Li et al., 2018

2001; Zhang et al., 2004). Based on the optimized terrace age model, Xu et al. (2005), Cowgill (2007), and Zhang et al. (2007) reinvestigated the key sites studied by Mériaux et al. (2004, 2005) and other sites with clear offsets and constrained the late Quaternary slip rates in the central part of the Altyn Tagh fault at 8–12 mm/yr (Table 1), which is consistent with the slip rates derived from GPS results (Zhang et al., 2007; Zheng et al., 2013). Zheng et al. (2013) integrated available GPS data and geological studies that demonstrate an eastward decrease in slip rates along the Altyn Tagh fault. Slip rates in the western and central sections of the Altyn Tagh fault vary within the range of 8–12 mm/yr, then decrease to 4–5 mm/yr in the junction zone with the Danghe Nan Shan, and drop to less than 2 mm/yr near the eastern end (Fig. 4) (Zhang et al., 2007; Jolivet et al., 2008; Zheng et al., 2013). The distribution of slip rates shows that ~8 mm/yr of the left-slip rate in the Altyn Tagh fault is transferred into thrusting and folding in the western Qilian Shan.

The Haiyuan fault is another major left-lateral strike-slip fault in northeastern Tibet, extending for nearly 1000 km from ~98° E to ~106° E (Fig. 4) (Hetzel, 2013). By dating the abandonment age of displaced moraines, Lasserre et al. (1999) suggested that the left-lateral strike-slip rate is 12–20 mm/yr in the central segment, which supports relatively higher slip rates in the Haiyuan fault. Afterward, Zheng et al. (2013) reanalyzed these sites and noted that the data sampling positions and measured displacements are disputable. Yao et al. (2019) reevaluated the slip rates at two sites studied by Lasserre et al. (1999) and derived a slip rate of 5.0–8.9 mm/yr. More recently, most of the studies have demonstrated lower slip rates along the major slip segments, varying in the range of 4–6 mm/yr (Table 1) (Zheng et al., 2013; Yao et al., 2019; Liu et al., 2022), in agreement with the GPS results (Zheng et al., 2013; Huang et al., 2022). Both geomorphological and geodetic studies reveal that the slip rates remain stable in the central part and decrease rapidly at the terminations (Fig. 4) (Zheng et al., 2013; Huang et al., 2022; Liu et al., 2022). The slip rate is only 1–2 mm/yr at the western end of the Haiyuan fault, increases to ~4 mm/yr in the Lenglongling segment, then remains 4–6 mm/yr in the range of 500 km in the middle section, and decreases to about 2 mm/yr at the eastern end of the fault (Fig. 4).

The NWW-trending thrust faults

The main structural direction of the Qilian Shan is west-northwest, along which a series of band-shaped mountain ranges and subparallel thrust faults is developed. The strike of these thrusts is N60°–70° W (Fig. 4) (Chen et al., 2022), approximately perpendicular to the collision direction between India and Eurasia. From north to south, five large-scale NWW-trending thrust faults are distributed in the western Qilian Shan, that is, the North Qilian, Changma, Shule Nan Shan, Danghe Nan Shan, and North Qaidam faults (Fig. 4). In the eastern Qilian Shan, only a limited number of thrust faults have been investigated, such as the Qinghai Nan Shan and Laji Shan faults (Fig. 4). To study the strain distribution of the crustal shortening in the Qilian

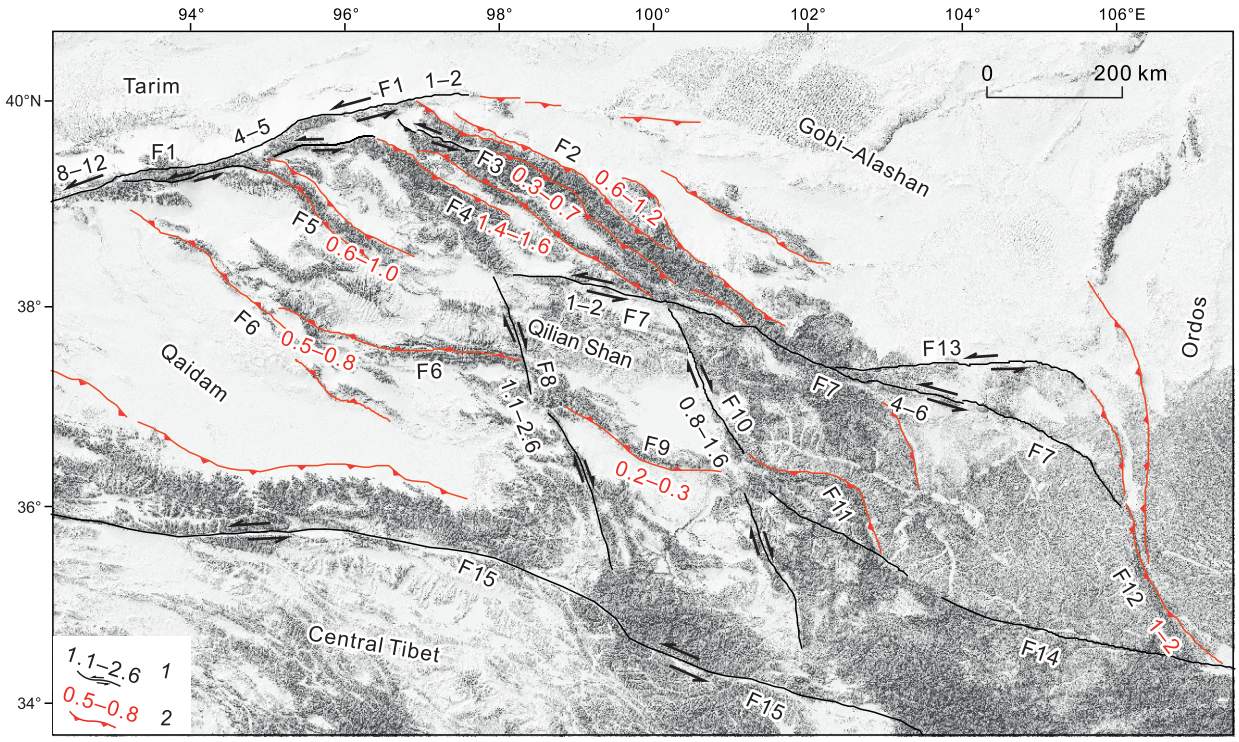

Fig. 4. Main active faults and their slip rates in the Qilian Shan. The black lines and numbers denote the strike-slip faults and their slip rates (mm/yr). The red lines and numbers denote thrust faults and their shortening slip rates (mm/yr). References to slip rates are shown in Table 1. Fault names: F1 – Altyn Tagh fault; F2 – North Qilian fault; F3 – Changma fault; F4 – Shule Nan Shan fault; F5 – Danghe Nan Shan fault; F6 – North Qaidam fault; F7 – Haiyuan fault; F8 – Ela Shan fault; F9 – Qinghai Nan Shan fault; F10 – Riyue Shan fault; F11 – Laji Shan fault; F12 – Liupan Shan fault; F13 – Gulang fault; F14 – West Qinling fault; F15 – East Kunlun fault.

Shan, the slip rates of the thrust faults have been extensively studied. GPS data show that the Qilian Shan absorbs the crustal shortening of 5–7 mm/yr (Zhang et al., 2004). However, because of the lack of GPS stations within the Qilian Shan, the amount of crustal shortening absorbed by each fault remains largely unknown.

Offset alluvial fans and river terraces along mountain fronts within the Qilian Shan provide opportunities to qualify the long-term slip rates of the thrust faults. By measuring the displacements of the geomorphologic markers and dating their initiation ages, the vertical slip rate and shortening rate of the North Qilian fault are estimated to be 0.8–1.4 mm/yr and 1–2 mm/yr. (Yang et al., 2018; Hetzel et al., 2019; Chen et al., 2022). The spatial distribution of slip rates of the North Qilian fault shows that the shortening rates in the central section are slightly greater than that at the two ends (Yang et al., 2018). The vertical slip rates of the Changma fault vary from 0.6 ± 0.2 mm/yr in the west to 0.3 ± 0.1 mm/yr in the middle (Luo et al., 2013; Chen et al., 2022). Hu et al. (2021) estimated a vertical slip rate of 1.5 ± 0.1 mm/yr and a shortening rate of 0.9 ± 0.1 mm/yr in the eastern section of the Shule Nan Shan fault. Using ^{10}Be exposure dating on displaced river terraces, the Danghe Nan Shan fault shows a vertical slip rate of 0.6 ± 0.2 mm/yr and a shortening rate of 0.8 ± 0.2 mm/yr (Xu et al., 2021). Likewise, the shortening rate of the North Qaidam fault has been estimated to be 0.5–0.8 mm/yr (Shao et al., 2019; Zhang et al., 2022). Based on the high-resolution topography and geomorphological dating, the vertical slip rate of the Qinghai Nan Shan fault is constrained to be 0.20 ± 0.03 mm/yr (Chen et al., 2021). The shortening rate of the Laji Shan fault is about 1.8 mm/yr (Li et al., 2018). The widely distributed shortening rates in the western Qilian Shan demonstrate diffuse crustal shortening (Fig. 4). The number of thrust faults and their shortening rates in the eastern Qilian Shan are significantly smaller and lower than those in the western Qilian Shan.

In the junction zones between the western Qilian Shan and the Altyn Tagh fault, the above-mentioned NWW thrust faults deflect southward. Among them, the strikes of the Danghe Nan Shan, Shule Nan Shan, and Changma faults bend southward from NWW to SWW in their western segments; then they are connected with the Altyn Tagh fault (Fig. 4). The field investigations of the deformed landforms suggest a left-lateral slip rate of 1.4–3.7 mm/yr in the western section of the Changma fault (Luo et al., 2013; Du et al., 2019) and a left-lateral slip rate of 2.0–2.8 mm/yr in the western segment of the Shule Nan Shan fault (Luo et al., 2015). The left-lateral slip rate in the western segment of the Danghe Nan Shan fault is estimated to be 4–5 mm/yr (Fig. 4) (Liu et al., 2020). Although there is a slight amount of southward bending in the western sections of the North Qil-

ian and North Qaidam faults, no obvious left-lateral strike-slip has been observed (Hetzel, 2013; Chen et al., 2022).

The NNW-trending strike-slip faults

There are two large right-lateral strike-slip faults in the interior of the Qilian Shan, the Ela Shan and Riyue Shan faults, distributed in the NNW orientation between the Kunlun and Haiyuan faults (Fig. 4). The right-lateral strike-slip activity accommodates the relative displacements between adjacent blocks. By combining terrace riser offsets with terrace ages dated by ^{14}C, optically stimulated luminescence, and ^{10}Be techniques, Yuan et al. (2011) determined the long-term average strike-slip faults to be 1.1 ± 0.3 mm/yr and 1.2 ± 0.4 mm/yr for the Ela Shan and Riyue Shan faults, respectively (Fig. 4). Recently, Chen et al. (2021) have revisited the central segment of the Ela Shan fault and reestimated the right-lateral strike-slip rate to be 2.6 ± 1.2 mm/yr. Additionally, GPS measurements suggest that the slip rates of the Ela Shan and Riyue Shan faults are ~1.6 and ~1.8 mm/yr (Li et al., 2018), which are slightly higher than the geological results by Yuan et al. (2011).

GPS CRUSTAL MOVEMENT VELOCITY FIELD

To investigate the regional crustal deformation, we developed a GPS-based crustal movement velocity field of the Qilian Shan with respect to stable Eurasia. This field is derived from GPS observation data collected over the past 20 years (Zheng et al., 2017b; Wang and Shen, 2020). Previous studies indicate that the entire Tibetan Plateau experiences crustal shortening of 36–40 mm/yr between India and Eurasia, of which only 5–7 mm/yr is accommodated by the Qilian Shan (Zhang et al., 2004). The GPS velocity vectors in the Qilian Shan point to the northeast, aligning with the overall northward movement orientation of the Indian Plate. Notably, the crustal shortening is more significant in the western Qilian Shan, because the GPS velocity vectors in this area consistently maintain a north-northeastward (NNE) orientation, with a gradual decrease (Fig. 5). At the same time, in the eastern Qilian Shan, the magnitudes of the GPS velocity vectors not only undergo noticeable changes but also exhibit a clockwise rotation. As depicted in Fig. 5, the GPS velocity vectors in the eastern Qilian Shan indicate a northeastward movement in the Qinghaihu block, an eastward movement in the Xining block, and a southeastward movement in the Lanzhou block.

To illustrate the amount of crustal shortening in the western and eastern Qilian Shan regions, we constructed two velocity profiles: A–A′ and B–B′, which extend across the Qilian Shan (Figs. 5, 6*A*, *B*). Profile A–A′ demonstrates a significant decrease in the N30° E velocity component across the western Qilian Shan, from south to north. In the southern Qilian Shan, the N30° E velocity component reaches 8–10 mm/yr, while in the northern Qilian Shan, it is approximately 4 mm/yr. As the profile crosses the mountain ranges of the northern Qilian Shan and extends into the

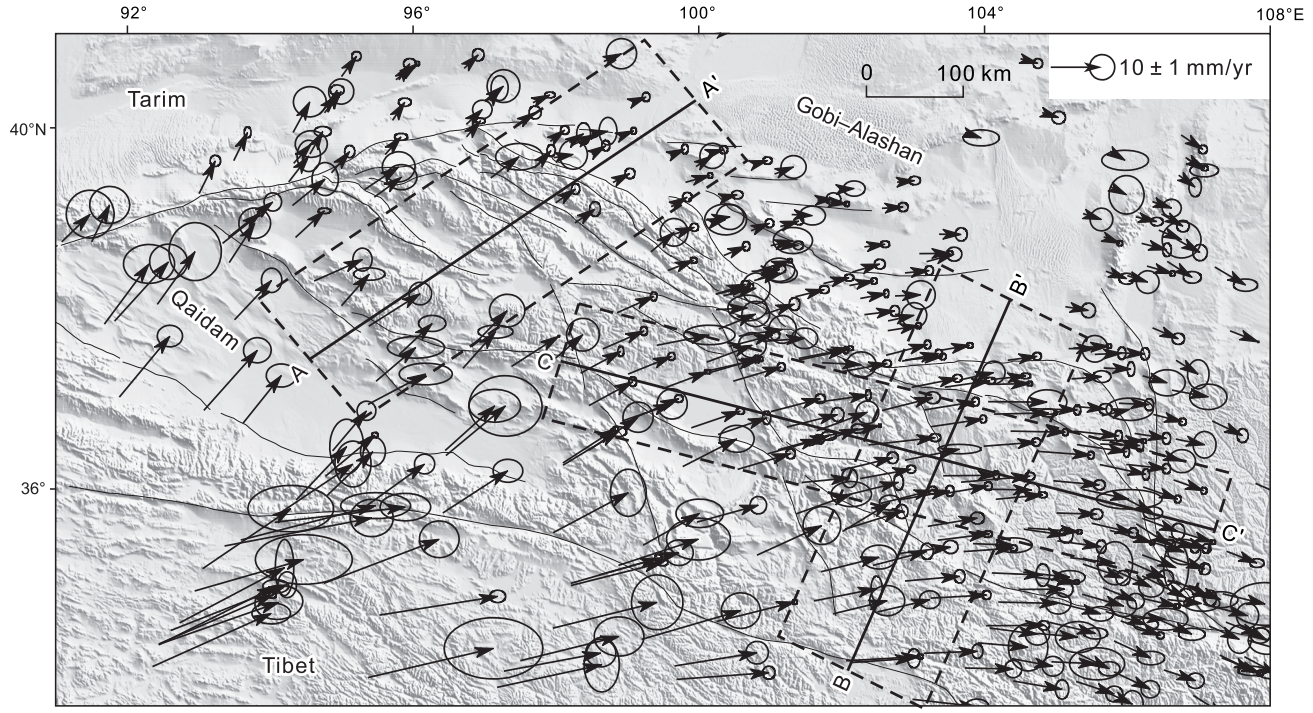

Fig. 5. The GPS crustal movement velocity field of the Qilian Shan with respect to stable Eurasia with 95% confidence ellipses. The black arrows show the GPS stations and velocity vectors transformed by Zheng et al. (2017b).

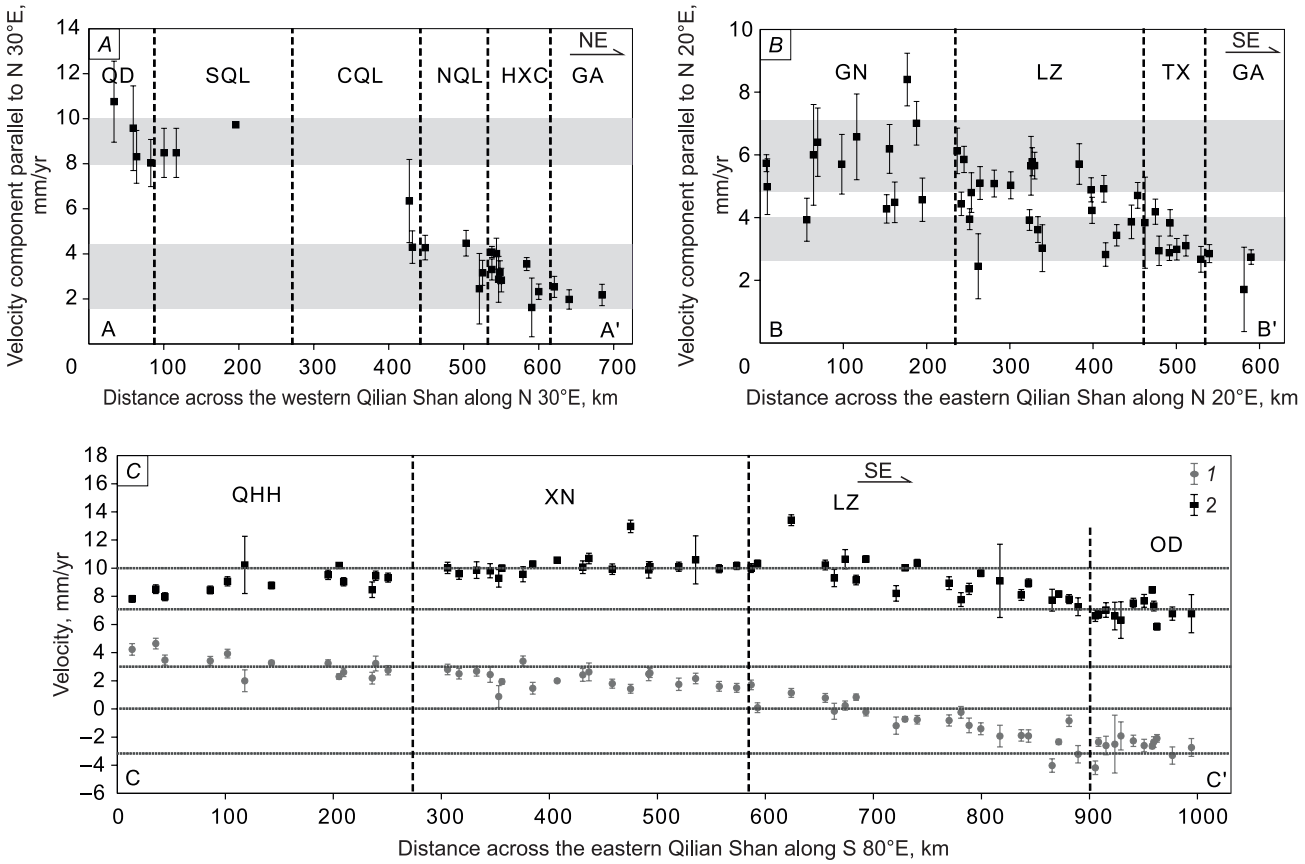

Fig. 6. GPS velocity profiles across the Qilian Shan. *A* – Profile A–A′ across the western Qilian Shan along N30 °E; *B* – profile B–B′ across the eastern Qilian Shan along N20° E; *C* – profile C–C′ across the eastern Qilian Shan along S80° E. Velocity vectors in profile C–C′ are divided into the eastward velocity and northward velocity components, *1* – eastward velocity component, *2* – northward velocity component. In the northward component, positive numbers denote northward; negative numbers, southward. In the eastward component, positive numbers denote eastward; negative numbers, westward. The locations of the profiles are shown in Fig. 5. Abbreviations: QD – Qaidam basin; SQL – South Qilian block; CQL – Central Qilian block; NQL – North Qilian block; HXC – Hexi Corridor block; GA – Gobi–Alashan block; GN – Gannan block; LZ – Lanzhou block; TX – Tongxin block; QHH – Qinghaihu block; XN – Xining block; OD – Ordos block.

Gobi–Alashan block, the velocity component diminishes to only 2–3 mm/yr (Figs. 5, 6*A*). Thus, the crustal shortening in the western Qilian Shan amounts to 5–7 mm/yr, which aligns with previous results (Zhang et al., 2004).

Profile B–B′ reveals that the N20° E velocity component in the eastern Qilian Shan does not exhibit a significant decrease, as observed in the western Qilian Shan. In the southern section of the profile, the N20° E velocity component is 5–7 mm/yr, while in the northern part, it varies in the range of 3–4 mm/yr (Figs. 5, 6*B*). Consequently, the crustal shortening in the eastern Qilian Shan amounts to only 2–3 mm/yr, which is, approximately, half the crustal shortening as observed in the western Qilian Shan.

Despite the lesser magnitude of crustal shortening in the eastern Qilian Shan compared to that in the western Qilian Shan, the GPS velocity field indicates notable eastward movement and clockwise rotation in the eastern Qilian Shan. Therefore, we generated profile C–C′, which extends in an approximately east–west direction across the eastern Qilian Shan, and decomposed the velocity into northward and eastward components (Figs. 5, 6*C*). The eastward velocity component shows a variation from 8 to 10 mm/yr (Fig. 6*C*). If we compare it with the eastward velocity component of 2–3 mm/yr observed in the northern Gobi–Alashan basin, the eastward velocity in the eastern Qilian Shan relative to that in the northern Gobi–Alashan block amounts to 5–7 mm/yr (Figs. 5, 6*C*). Furthermore, the eastward velocity component remains relatively constant at around 10 mm/yr within a distance of 500 km along the middle of profile C–C′, which is slightly higher than the rates at the eastern and western ends (Fig. 6*C*). In contrast to the relatively stable eastward velocity component, the northward velocity component exhibits a noticeable gradient decrease. On profile C–C′, the northward velocity component is 3–4 mm/yr in the Qinghaihu block and 0–2 mm/yr in the Xining block. Subsequently, the northward velocity component begins to pass into negative values in the Lanzhou block, reaching –2 to –3 mm/yr in the southeastern part of the Lanzhou block (Fig. 6*C*). This indicates that the crust starts to move southward. The variation in the northward velocity component

suggests a distinct clockwise rotation of the crust in the eastern Qilian Shan, shifting from a northward velocity of 3–4 mm/yr in the Qinghaihu block to a southward velocity of 2–3 mm/yr in the Lanzhou block (Figs. 5, 6*C*).

DISCUSSION

Tectonic deformation characteristics of the Qilian Shan and the deformation pattern

The results inferred from regional seismicity, faulting, and GPS crustal movement field consistently suggest that the active tectonic deformation of the Qilian Shan is primarily characterized by the NNE-oriented crustal shortening coupled with the eastward extrusion and clockwise rotation of crustal material in response to India–Eurasia convergence (Fig. 7). Specifically, the western Qilian Shan is dominated by the NNE-oriented crustal shortening and thickening, manifested as the predominant compression-type earthquakes, thrust faults, and decrease in GPS velocities. Conversely, the eastern Qilian Shan is mainly characterized by the eastward extrusion and clockwise rotation of blocks, supported by the shear-type seismic events, rapid strike-slip of boundary faults, and eastward movement and clockwise deflection of GPS velocity vectors. The crustal shortening rate in the western Qilian Shan is 5–7 mm/yr, significantly higher than that observed in the eastern Qilian Shan (2–3 mm/yr) (Fig. 7). The shortening rate difference between the western and eastern Qilian Shan is more likely to be accommodated by the right-lateral strike-slip of the Ela Shan and Riyue Shan faults, because the total strike-slip rate of these two faults is 3–4 mm/yr (Yuan et al., 2011; Chen et al., 2021), nearly compensating for the disparity in crustal shortening rates between the western and eastern Qilian Shan. The eastward velocity of the eastern Qilian Shan reaches 5–7 mm/yr relative to that in the Gobi–Alashan block to the north (Fig. 7), which is generally consistent with the late Quaternary slip rate of the Haiyuan fault (Zheng et al., 2013; Liu et al., 2022). This suggests that the Haiyuan fault plays a significant role as a boundary fault, guiding the eastward movement of blocks in the eastern Qilian Shan along the large longitudinal strike-slip faults (Trifonov et al., 2021). The decrease in GPS velocity at the eastern margin of the Qilian Shan and strike-slip rate along the eastern segment of the Haiyuan fault is mainly attributable to the blocking of the Ordos Basin to the east. As a result, there is a transition from shear strain along the Haiyuan fault to contraction strain in the Liupan Shan fault (Fig. 7) (Zheng et al., 2013; Li et al., 2018; Liu et al., 2022).

The mentioned deformation pattern of the Qilian Shan is supported by the strain rate fields of the Qilian Shan (Zheng et al., 2017b; Li et al., 2018; Pan et al., 2020). Pan et al. (2020) constructed two-dimensional strain rate fields of the Qilian Shan based on the GPS velocity field, which include principal strain rate, maximum shear strain rate, rotational strain rate, and dilatational strain rate. The principal and dilatation strain rates indicate that NNE-oriented contraction is prevalent throughout the western Qilian Shan (Pan et al., 2020). High maximum shear strain rates are primarily concentrated along the Altyn Tagh, Haiyuan, and Ela Shan faults, suggesting that shear deformation is centralized in these major boundary strike-slip faults (Pan et al., 2020). The rotational strain rate exhibits a slight counterclockwise rotation in the western Qilian Shan, which is deemed to be the impact of left-lateral strike-slip motion in the transition

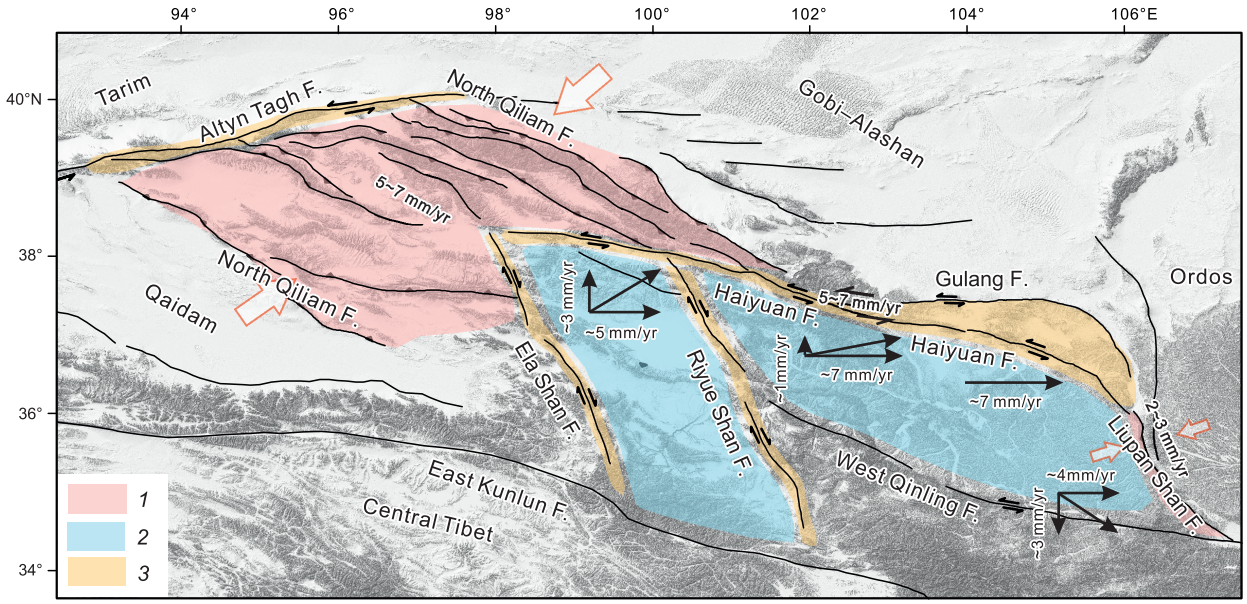

Fig. 7. The deformation pattern of the Qilian Shan. The western Qilian Shan is characterized by distributed crustal shortening, while the eastern Qilian Shan is characterized by blocklike eastward extrusion along major strike-slip faults coupled with clockwise rotation of blocks. *1* – compression area, *2* – block-like area, *3* – shearing area.

zone (Zheng et al., 2013). In contrast, the rotational strain rate shows an obvious clockwise rotation in the eastern Qilian Shan, between the Haiyuan and East Kunlun faults, which is generally consistent with the GPS velocity field presented in this study (Pan et al., 2020). These strain rates explicitly illuminate the spatial variation of regional strain and quantitatively support the deformation pattern proposed in this study.

In addition to crustal thickening and eastward extrusion modes, continuous or blocklike deformations are generally considered alternative geodynamic models to interpret crustal deformation resulting from continent–continent collision (Zhang et al., 2004). The former suggests that the crustal deformation is distributed or diffuse, while the latter indicates that the deformation is concentrated along the boundary faults of blocks and is inconspicuous in the block interiors. The distinction between them largely depends on lithospheric mechanic strength, which is associated with geologic structures, the early evolution of the Earth, rock rheology, and other factors (Royden et al., 2008). In this study, the tectonic deformation of the Qilian Shan can also be interpreted using these two models. Historical earthquakes and active faults are widespread in the western Qilian Shan, particularly in the Central and North Qilian blocks (Figs. 3, 4). In contrast, earthquakes and active faults are primarily located along the block boundaries in the eastern Qilian Shan, such as the Haiyuan and Ela Shan faults (Figs. 3, 4). Therefore, we suggest that the continuous deformation characterizes the crustal deformation of the western Qilian Shan, whereas the blocklike deformation matches the eastern Qilian Shan. Considering these two deformation modes, the deformation pattern can be optimized, indicating that the western Qilian Shan is characterized by distributed north–south crustal shortening, while the eastern Qilian Shan exhibits blocklike eastward extrusion along major strike-slip faults coupled with clockwise rotation of blocks.

Implications for geodynamics of the Tibetan Plateau

Crustal shortening appears to be the main mode for accommodating the India–Eurasia convergence. The GPS velocity gradient indicates that the crustal shortening across the Tibetan Plateau decreases linearly from south to north (Wang et al., 2001; Zhang et al., 2004). Apart from the Qilian Shan, another significant region experiencing north–south crustal shortening is the Himalayan thrust belt on the southern margin of the Tibetan Plateau. The shortening rate inferred from GPS data across the Himalayas reaches 15–20 mm/yr, accounting for 40–50% of the 36–40 mm/yr convergence between India and Eurasia (Fig. 8*A*) (Zhang et al., 2004). The principal strain rate demonstrates the highest compressive strain oriented in the north–south direction in the Himalayas (Wu et al., 2020). Furthermore, typical contraction structures, such as thrust faults and folds, are predominantly located on the southern and northeastern margins of the plateau. However, the vast interior of the plateau is characterized by normal and strike-slip faulting rather than contraction deformation. This discrepancy appears to be inconsistent with the overall compression tectonic background of the Tibetan Plateau. Therefore, how central Tibet deforms in response to the India–Eurasia convergence is a controversial issue (Wang et al., 2001).

One of the most intriguing tectonic activities occurring in Tibet is the crustal lateral extrusion and east–west extension in the central plateau. Three large-scale strike-slip faults, including the Jiali, Xianshuihe, and East Kunlun faults from south to north (Fig. 8*A*), are distributed in central Tibet along the east–west direction, indicating significant shear deformation occurring in this vast region (Hetzel, 2013). North–south-trending normal faults and grabens due to east–west extension are widely distributed in the central and western plateau (Fig. 8*A*) (Tapponnier et al., 1981). The GPS velocities present the eastward movement in the eastern plateau, which suggests that tectonic deformation in this region is characterized by large-scale eastward extrusion of the plateau materials and the clockwise rotation around the eastern Himalayan syntaxis (Fig. 8*A*) (Wang et al., 2001; Zhang et al., 2004; Wang and Shen, 2020). The GPS velocity component perpendicular to the India–Eurasia convergence direction increases steadily northward from the Himalayas, peaks at ~20 mm/yr between the Jiali and Xianshuihe faults, and then decreases rapidly northward as a result of left-lateral slip on the Xianshuihe and East Kunlun faults (Fig. 8*B*) (Wang et al., 2001; Zhang et al., 2004). The eastward extrusion rate of ~20 mm/yr at 95° E and the westward rate of ~6 mm/yr at 80° E indicate an extension rate of 22 ± 3 mm/yr across the central plateau (Fig. 8*A*) (Zhang et al., 2004; Wang and Shen, 2020). The above results clearly show that the large-scale lateral movement and east–west extension may be responsible for the crustal shortening in central Tibet in spite of a lack of thrust faults. Moreover, the right-lateral strike-slip of the Jiali fault and the rapid left-lateral strike-slip of the Xianshuihe and East Kunlun faults determine the main region of the lateral extrusion and extension (Zhang et al., 2004; Gan et al., 2007). The slip rates of these strike-slip faults reveal the rate difference of the eastward movement of blocks in central Tibet (Zhang et al., 2004). Besides, the Longmen Shan on the eastern margin of the Tibetan Plateau underwent significant east–west compression (Fig. 8*A*). It is assumed that the uplift and thrusting of the eastern margin of Tibet are attributed to the blocking of the Sichuan basin when the central plateau extrudes eastward (Wang et al., 2001; Zhang et al., 2004).

The driving mechanism of east–west extension and eastward extrusion in central Tibet largely depends on the understanding of the deep crustal structure. Geological investigations and space geodetic monitoring can only depict the structure of the upper crust or subsurface, and it is difficult to provide effective constraints for the lower crust. Seismic tomography and magnetotelluric imaging permit studying the deep structure and mechanical state of the lower crust, which could be characterized by a reduced seismic velocity

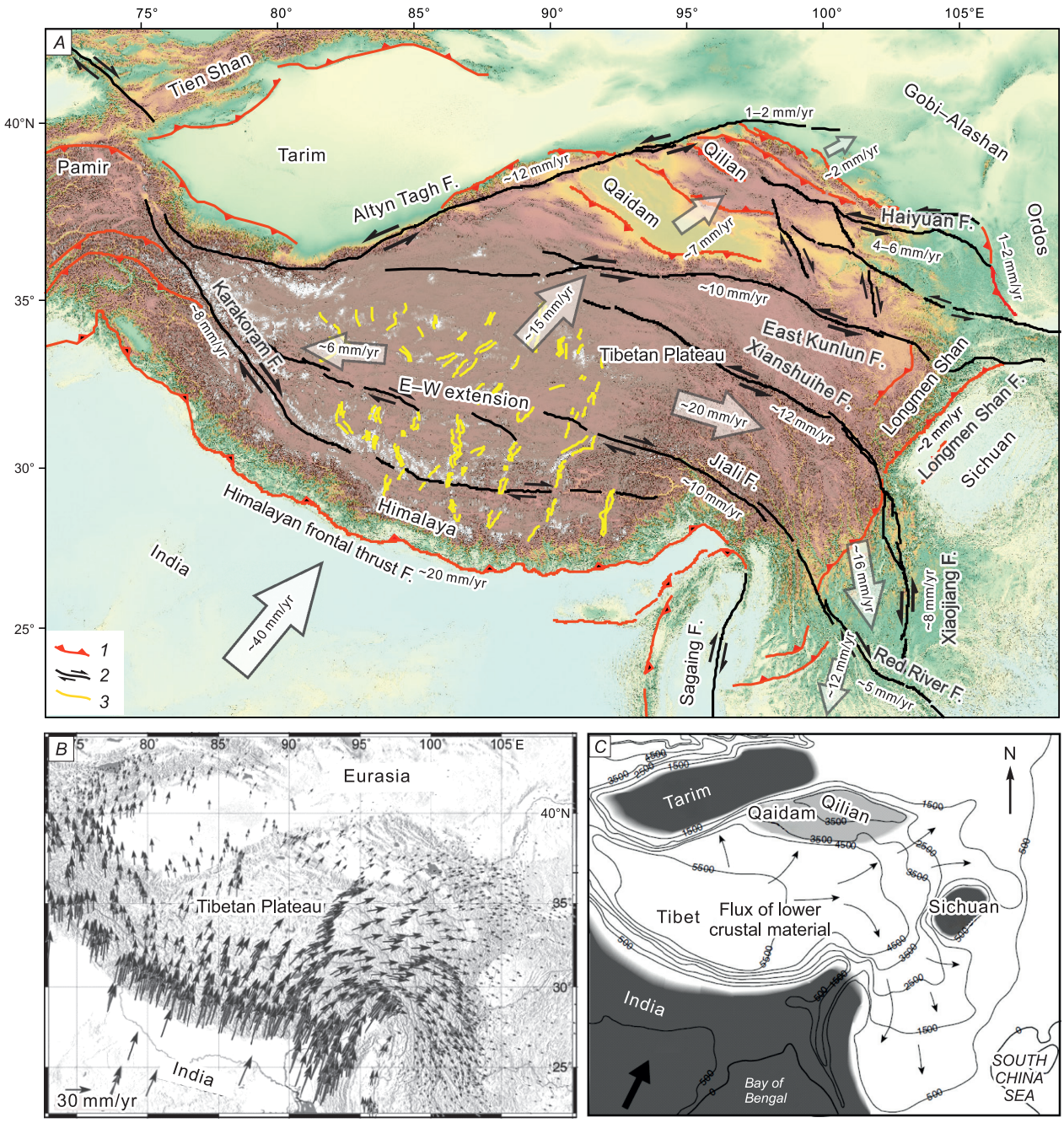

Fig. 8. Tectonic deformation of the Tibetan Plateau. *A* – Simplified tectonic map of the Tibetan Plateau showing active faults, fault slip rates, and crustal movements. The crustal movement rates and fault slip rates were derived from the data of Zhang et al. (2004) and Wang and Shen (2020), *1* – thrust fault, *2* – strike-slip fault, *3* – normal fault. *B* – the GPS crustal movement velocity field of the Tibetan Plateau relative to stable Eurasia, modified from Gan et al. (2007); *C* – the topographic contour of smoothed elevations of the Tibetan Plateau showing the outward movements of deep crustal flow, with a contour interval of 1000 m, modified from Clark and Royden (2000).

and an elevated electrical conductivity (reduced resistivity) (Royden et al., 2008), as compared with rigid continental crust (Bai et al., 2010). Surface-wave tomography and receiver-function analysis from regional seismic arrays in eastern and central Tibet show a lower crust with low shear-wave speed and, presumably, low mechanical strength (Kind et al., 2002; Yao et al., 2008). Magnetotelluric data from central Tibet present wide spread of anomalous conductivity, indicating a hot, fluid-rich middle and lower crust within the central plateau, which points to a relatively weaker lithosphere (Wei et al., 2001). These results support the lower crustal flow model proposed by Royden et al. (1997) and Clark and Royden (2000), which assumes that the ductile lower crustal flow with low viscosity in the central plateau is decoupled from the upper crust and extrudes toward the plateau margins (Fig. 8*C*) (Clark and Royden, 2000). Enlight-

ened by this model, Bai et al. (2010) utilized magnetotelluric exploration to detect two major zones or channels of high electrical conductivity beneath the southeastern Tibetan Plateau, suggesting that the lower crustal flow extends horizontally from the central plateau into southwestern China. However, on the eastern margin of the Tibetan Plateau along the Longmen Shan, the east-moving lower crustal flow is blocked by the Sichuan basin. The seismic tomography shows that this basin appears to be a deeply rooted, mechanically strong unit underlain by cratonlike lithosphere (Royden et al., 2008). Therefore, the resistance to the eastward flow of the lower crust builds a steep topographic margin in the eastern plateau that is even steeper than the Himalayan front (Clark and Royden, 2000). Moreover, Royden et al. (2008) speculated that the east–west extension, the eastward movement of the central plateau, the rapid uplift of the eastern margin, and the establishment of the modern deformation regime in central Tibet are all the result of the underlying lower crustal flow out of the plateau.

The questions whether the lower crustal flow extruding outward from the central plateau also affects the northeastern margin of the Tibetan Plateau and whether it determines the tectonic deformation pattern of the Qilian Shan are still subject to debate. In recent years, numerous geophysical explorations have been carried out to highlight the deep crustal structure of the Qilian Shan. Based on the observation data from seismic arrays, Li et al. (2022) derived the intracrustal structure in the Qilian Shan and revealed the structural difference between the western and eastern Qilian Shan, showing that there is a low-velocity zone at a depth of 20–40 km in the western Qilian and no low-velocity observation at the same level in the eastern Qilian. This difference indicates that the western Qilian Shan has a relatively weaker middle crust, which is deemed to be the result of the crustal shortening and thickening (Xia et al., 2021), while the eastern Qilian Shan is characterized by relatively uniform high-velocity crust, which behaves as a relatively rigid lithosphere (Li et al., 2022), in agreement with the tectonic deformation pattern inferred from this study. In addition, the teleseismic receiver functions and gravity data show that the crustal thickness gradually decreases eastward from ~65 km beneath the western Qilian to ~50 km in the Lanzhou block (Shi et al., 2022), indicating that the crustal shortening in the western Qilian Shan is greater than that in the eastern Qilian Shan. Likewise, in the lower crust and upper mantle lithosphere under the northeastern plateau, seismic explorations suggest strong and rigid lower crusts under the Qaidam, Gobi–Alashan, and Ordos blocks (Shen et al., 2017; Yang et al., 2019). In contrast, under the eastern Qilian Shan, the lower crust and upper mantle show weak and diffuse negative velocity gradients, which may be explained by elevated temperature and the presence of partial melts or by the interaction of the lateral lower crustal flow (Shen et al., 2017). This suggests that the eastern Qilian Shan may host an important channel for guiding the lower crustal flow to extrude outward. In the model of Royden et al. (1997, 2008) and Clark and Royden (2000), the bounding rigid blocks around the plateau, including the Sichuan, Ordos, Qaidam, Gobi–Alashan, and Tarim blocks, inhibit the flow of lower crustal material from the central plateau and, therefore, cause the formation of the boundary mountain ranges and outward extrusion of the crustal material along the northeastern and southeastern margins of the Tibetan Plateau.

The outward extrusion of crustal material from central Tibet may systematically induce many tectonic events occurring within and around the Tibetan Plateau, such as the east–west extension in the central plateau, crustal eastward extrusion and clockwise rotation on the southeastern margin, rapid surface uplift of the Longmen Shan on the eastern margin, formation and tectonic deformation of the Qilian Shan on the northeastern margin, etc. Numerous studies indicate that the initiation ages of these tectonic events exhibit approximate synchronization in the middle Miocene. Low-temperature thermochronological data suggest that the onset ages of normal faulting and east–west extension in central Tibet range from 12 Ma to 8 Ma (Sundell et al., 2013; Woodruff et al., 2013), in rough agreement with other constrained ages (Yin and Harrison, 2000; Royden et al., 2008). The Xianshuihe fault in the eastern plateau is a key structure accommodating the eastward movement of crustal materials, and Roger et al. (1995) constrained the initiation of slip on this fault to be 12–10 Ma. The distortion of the Red River fault and the Yalong–Yulong–Longmen Shan thrust belt formed as the result of eastward movement and clockwise rotation of crust around the southeastern margin of the plateau, and Gan et al. (2021) infer that this pattern of deformation developed since 10.1 ± 1.5 Ma, which is approximately synchronous with slip reversal of the Red River fault and rapid river incision in southeastern Tibet (Clark et al., 2005; Fyhn and Phach, 2015). Thermochronology and thermal models suggest rapid exhumation starting at 12–10 Ma in the Longmen Shan, which marks the onset of surface uplift of the eastern margin of the plateau (Kirby et al., 2002; Wang et al., 2012). Similarly, the estimated initiation of uplift of the Qilian Shan is constrained to be 14–8 Ma based on apatite fission track chronology and magnetostratigraphy (Wang et al., 2017; Zheng et al., 2017a). These approximately synchronous events indicate that the extrusion of crustal material and the uplift of boundary mountain ranges in Tibet were probably initiated during the middle Miocene (14–8 Ma). The uplift and tectonic deformation of the Qilian Shan might be a portion of the outward expansion of the Tibetan Plateau since the middle Miocene.

CONCLUSIONS

The active tectonic deformation of the Qilian Shan has been investigated using regional seismic records, active fault data, slip rates, and GPS velocity measurements collected over the past two decades. Our results suggest that the

western Qilian Shan is characterized by distributed north–south crustal shortening, manifested principally as the diffuse spatial distribution of compression earthquakes and thrust faults, as well as a significant decrease in GPS velocities along the NNE direction, while the eastern Qilian Shan is dominated by blocklike eastward extrusion along major strike-slip faults coupled with clockwise rotation of blocks, specified in earthquakes and strike-slip faults along the major boundary faults and the eastward movement and clockwise rotation of GPS velocities. The north–south crustal shortening and lateral extrusion, two modes in response to the India–Eurasia convergence, also match the northeastern margin of the Tibetan Plateau. The tectonic deformation of the western Qilian Shan is largely in agreement with the former, while the eastern Qilian Shan corresponds closely to the latter. The deep crustal structure beneath the Tibetan Plateau indicates that the lower crustal materials with low viscosity flowing outward from the central plateau may drive the outward extrusion of crust and the growth of many mountain ranges bounding the Tibetan Plateau. A suite of tectonic events associated with the outward growth of the plateau was initiated approximately during the middle Miocene (14–8 Ma). The uplift and tectonic deformation of the Qilian Shan might be a portion of the outward expansion of the Tibetan Plateau since the middle Miocene.

ACKNOWLEDGMENTS AND FUNDING

The authors are grateful to the National Earthquake Data Center in China (data.earthquake.cn), CENC (www.ceic.ac.cn), and GCMT (www.globalcmt.org) for providing the earthquake data for this study. We thank the Crustal Movement Observation Network of China (CMONOC) for sharing the GPS data sets. We sincerely thank the reviewers for their helpful suggestions and constructive comments. This research was financially supported by the China Scholar Council (CSC).

REFERENCES

Bai, D., Unsworth, M.J., Meju, M.A., Ma, X., Teng, J., Kong, X., Sun, Y., Sun, J., Wang, L., Jiang, C., Zhao, C., Xiao, P., Liu, M., 2010. Crustal deformation of the eastern Tibetan plateau revealed by magnetotelluric imaging. Nat. Geosci. 3, 358–362, doi: 10.1038/ngeo830.

Burtman, V.S., 2012. Geodynamics of Tibet, Tarim, and the Tien Shan in the Late Cenozoic. Geotectonics 46 (3), 185–211, doi: 10.1134/S0016852112030028.

Chen, G., Ai, M., Zheng, W., Bi, H., Liu, J., Zhang, Y., Ge, W., Zhang, D., Huang, R., 2021. Nonrigid bookshelf kinematics of Northeastern Tibet: Constraints from fault slip rates around the Qinghai Lake and Chaka-Gonghe basins. Lithosphere Spec. 2, 4115729, doi: 10.2113/2021/4115729.

Chen, Z., Xu, W., Liu, R., Li, A., Koronovsky, N.V., 2022. Tectonic deformation of the Western Qilian Shan in response to the north-south crustal shortening and sinistral strike-slip of the Altyn Tagh fault inferred from geomorphologic data. Front. Earth Sci. 10, 808935, doi: 10.3389/feart.2022.808935.

Clark, M.K., Royden, L.H., 2000. Topographic ooze: Building the eastern margin of Tibet by lower crustal flow. Geology 28, 703–706, doi: 10.1130/0091-7613(2000)28<703:TOBTEM>2.0.CO;2.

Clark, M.K., House, M.A., Royden, L.H., Whipple, K.X., Burchfiel, B.C., Zhang, X., Tang, W., 2005. Late Cenozoic uplift of southeastern Tibet. Geology 33, 525–528, doi: 10.1130/G21265.1.

Cowgill, E., 2007. Impact of riser reconstructions on estimation of secular variation in rates of strike-slip faulting: Revisiting the Cherchen River site along the Altyn Tagh Fault, NW China. Earth Planet. Sci. Lett. 254, 239–255, doi: 10.1016/j.epsl.2006.09.015.

Deng, Q., 1996. Active tectonics in China [in Chinese with English abstract]. Geol. Rev. 42 (4), 295–299.

Ding, G., 1984. Active faults in China, in: A Collection of Papers of International Symposium on Continental Seismicity and Earthquake Prediction (ISCSEP). Seismol. Press, Beijing, pp. 225–242.

Du, J., Fu, B., Guo, Q., Shi, P., Xue, G., Xu, H., 2019. Segmentation and termination of the surface rupture zone produced by the 1932 *Ms* 7.6 Changma earthquake: New insights into the slip partitioning of the eastern Altyn Tagh fault system. Lithosphere 12, 19–39, doi: 10.1130/L1113.1.

Feng, W., He, X., Zhang, Y., Fang, L., Samsonov, S., Zhang, P., 2022. Seismic faults of the 2022 Mw 6.6 Menyuan, Qinghai earthquake and their implication for the regional seismogenic structures [in Chinese]. Chin. Sci. Bull. 68, 254–270, doi: 10.1360/TB-2022-0154.

Fyhn, M.B.W., Phach, P.V., 2015. Late Neogene structural inversion around the northern Gulf of Tonkin, Vietnam: Effects from right-lateral displacement across the Red River fault zone. Tectonics 34, 290–312, doi: 10.1002/2014TC003674.

Gan, W., Zhang, P., Shen, Z.-K., Niu, Z., Wang, M., Wan, Y., Zhou, D., Cheng, J., 2007. Present-day crustal motion within the Tibetan Plateau inferred from GPS measurements. J. Geophys. Res. 112, B08416, doi: 10.1029/2005JB004120.

Gan, W., Molnar, P., Zhang, P., Xiao, G., Liang, S., Zhang, K., Li, Z., Xu, K., Zhang, L., 2021. Initiation of clockwise rotation and eastward transport of Southeastern Tibet inferred from deflected fault traces and GPS observations. GSA Bull. 134, 1129–1142, doi: 10.1130/B36069.1.

Guo, X., Jiang, C., Han, L., Yin, H., Zhao, Z., 2022. Focal mechanism data set in Chinese mainland and its adjacent area (2009-2021) [EB/OL], doi: 10.12080/nedc.11.ds.2022.0004.

Hetzel, R., 2013. Active faulting, mountain growth, and erosion at the margins of the Tibetan Plateau constrained by in situ-produced cosmogenic nuclides. Tectonophysics 582, 1–24, doi: 10.1016/j.tecto.2012.10.027.

Hetzel, R., Hampel, A., Gebbeken, P., Xu, Q., Gold, R.D., 2019. A constant slip rate for the western Qilian Shan frontal thrust during the last 200 ka consistent with GPS-derived and geological shortening rates. Earth Planet. Sci. Lett. 509, 100–113, doi: 10.1016/j.epsl.2018.12.032.

Hu, X., Pan, B., Kirby, E., Gao, H., Hu, Z., Cao, B., Geng, H., Li, Q., Zhang, G., 2015. Rates and kinematics of active shortening along the eastern Qilian Shan, China, inferred from deformed fluvial terraces. Tectonics 34, 2478–2493, doi: 10.1002/2015TC003978.

Hu, X., Cao, X., Li, T., Mao, J., Zhang, J., He, X., Zhang, Y., Pan, B., 2021. Late Quaternary fault slip rate within the Qilian orogen, insight into the deformation kinematics for the NE Tibetan Plateau. Tectonics 40, e2020TC006586, doi: 10.1029/2020TC006586.

Huang, Z., Zhou, Y., Qiao, X., Zhang, P., Cheng, X., 2022. Kinematics of the ~1000 km Haiyuan fault system in northeastern Tibet from high-resolution Sentinel-1 InSAR velocities: Fault architecture, slip rates, and partitioning. Earth Planet. Sci. Lett. 583, 117450, doi: 10.1016/j.epsl.2022.117450.

Jolivet, R., Cattin, R., Chamot-Rooke, N., Lasserre, C., Peltzer, G., 2008. Thin-plate modeling of interseismic deformation and asymmetry across the Altyn Tagh fault zone. Geophys. Res. Lett. 35, L02309, doi: 10.1029/2007GL031511.

Kind, R., Yuan, X., Saul, J., Nelson, D., Sobolev, S.V., Mechie, J., Zhao, W., Kosarev, G., Ni, J., Achauer, U., Jiang, M., 2002. Seismic images of crust and upper mantle beneath Tibet: evidence for Eurasian plate subduction. Science 298, 1219–1221, doi: 10.1126/science.1078115.

Kirby, E., Reiners, P.W., Krol, M.A., Whipple, K.X., Hodges, K.V., Farley, K.A., Tang, W., Chen, Z., 2002. Late Cenozoic evolution of the eastern margin of the Tibetan Plateau: Inferences from $^{40}Ar/^{39}Ar$ and (U-Th)/He thermochronology. Tectonics 21, 1001, doi: 10.1029/2000TC001246.

Kreemer, C., Blewitt, G., Klein, E.C., 2014. A geodetic plate motion and Global Strain Rate Model. Geochem. Geophys. Geosyst. 15, 3849–3889, doi: 10.1002/2014GC005407.

Lasserre, C., Morel, P.H., Gaudemer, Y., Tapponnier, P., Ryerson, F.J., King, G.C.P., Métivier, F., Kasser, M., Kashgarian, M., Liu, B., Lu, T., Yuan, D., 1999. Postglacial left slip rate and past occurrence of M≥8 earthquakes on the Western Haiyuan Fault, Gansu, China. J. Geophys. Res. Solid Earth 104, 17633–17651, doi: 10.1029/1998JB900082.

Li, H., Pan, J., Sun, Z., Si, J., Pei, J., Liu, D., Marie-Luce, C., Wang, H., Lu, H., Zheng, Y., Li, C., 2021. Continental tectonic deformation and seismic activity: a case study from the Tibetan Plateau [in Chinese]. Acta Geol. Sin. 95 (1), 194–213, doi: 10.19762/j.cnki.dizhixuebao.2021051.

Li, H., Huang, X., Gao, R., Ye, Z., 2022. The lithospheric structure differences between the western and eastern Qilian in the northeastern Tibetan Plateau [in Chinese]. Chin. J. Geophys. 65 (5), 1581–1594, doi: 10.6038/cjg2022P0735.

Li, Y., Liu, M., Wang, Q., Cui, D., 2018. Present-day crustal deformation and strain transfer in northeastern Tibetan Plateau. Earth Planet. Sci. Lett. 487, 179–189, doi: 10.1016/j.epsl.2018.01.024.

Liu, J., Ren, Z., Zheng, W., Min, W., Li, Z., Zheng, G., 2020. Late Quaternary slip rate of the Aksay segment and its rapidly decreasing gradient along the Altyn Tagh fault. Geosphere 16, 1538–1557, doi: 10.1130/GES02250.1.

Liu, J., Ren, Z., Zhang, H., Li, C., Zhang, Z., Zheng, W., Li, X., Liu, C., 2022. Slip rates along the Laohushan fault and spatial variation in slip rate along the Haiyuan fault zone. Tectonics 41, e2021TC006992, doi: 10.1029/2021TC006992.

Liu-Zeng, J., Klinger, Y., Xu, X., Lasserre, C., Chen, G., Chen, W., Tapponnier, P., Zhang, B., 2007. Millennial recurrence of large earthquakes on the Haiyuan Fault near Songshan, Gansu Province, China. Bull. Seismol. Soc. Am. 97, 14–34, doi: 10.1785/0120050118.

Luo, H., He, W., Wang, D., Yuan, D., Shao, Y., 2013. Study on the slip rate of Changma fault in Qilian Mountains since late Pleistocene [in Chinese]. Seismol. Geol. 35, 765–777, doi: 10.3969/j.issn.0253-4967.2013.007.

Luo, H., He, W., Yuan, D., Shao, Y., 2015. Slip rate of Yema River–Daxue Mountain fault since the Late Pleistocene and its implications on the deformation of the northeastern margin of the Tibetan Plateau. Acta Geol. Sin. (Engl. Ed.) 89, 561–574, doi: 10.1111/1755-6724.12447.

Meng, W., Guo, X., Li, Y., Han, L., Zhang, C., 2022. Tectonic stress field and dynamic characteristics in the northeastern margin of the Tibetan Plateau [in Chinese]. Chin. J. Geophys. 65, 3229–3251, doi: 10.6038/cjg2022P0236.

Mériaux, A.S., Ryerson, F.J., Tapponnier, P., van der Woerd, J., Finkel, R.C., Xu, X., Xu, Z., Caffee, M.W., 2004. Rapid slip along the central Altyn Tagh Fault: Morphochronologic evidence from Cherchen He and Sulamu Tagh. J. Geophys. Res. Solid Earth 109, B06401, doi: 10.1029/2003JB002558.

Mériaux, A.S., Tapponnier, P., Ryerson, F.J., Xiwei, X., King, G., van der Woerd, J., Finkel, R.C., Haibing, L., Caffee, M.W., Zhiqin, X., Wenbin, C., 2005. The Aksay segment of the northern Altyn Tagh fault: Tectonic geomorphology, landscape evolution, and Holocene slip rate. J. Geophys. Res. Solid Earth 110, B04404, doi: 10.1029/2004JB003210.

Molnar, P., Tapponnier, P., 1975. Cenozoic tectonics of Asia: Effects of a continental collision. Science 189, 419–426, doi: 10.1126/science.189.4201.419.

Pan, Z., Yun, Z., Shao, Z., 2020. Contemporary crustal deformation of Northeast Tibet from geodetic investigations and a comparison between the seismic and geodetic moment release rates. Phys. Earth Planet. Inter. 304, 106489, doi: 10.1016/j.pepi.2020.106489.

Peltzer, G., Tapponnier, P., Armijo, R., 1989. Magnitude of late Quaternary left-lateral displacements along the north edge of Tibet. Science 246, 1285–1289, doi: 10.1126/science.246.4935.1285.

Roger, F., Calassou, S., Lancelot, J., Malavieille, J., Mattauer, M., Xu, Z., Hao, Z., Hou, L., 1995. Miocene emplacement and deformation of the Konga Shan granite (Xianshui He fault zone, west Sichuan, China): Geodynamic implications. Earth Planet. Sci. Lett. 130, 201–216, doi: 10.1016/0012-821X(94)00252-T.

Royden, L.H., Burchfiel, B.C., King, R.W., Wang, E., Chen, Z., Shen, F., Liu, Y., 1997. Surface deformation and lower crustal flow in Eastern Tibet. Science 276, 788–790, doi: 10.1126/science.276.5313.788.

Royden, L.H., Burchfiel, B.C., van der Hilst, R.D., 2008. The geological evolution of the Tibetan Plateau. Science 321, 1054–1058, doi: 10.1126/science.1155371.

Shao, Y., Li, Z., Zhang, B., Wang, P., Yuan, D., Wu, M., 2019. Paleoseismological study of the southern Zongwulong Shan fault, Qilian Mountains, western China. Geomorphology 326, 107–115, doi: 10.1016/j.geomorph.2017.12.036.

Shen, X., Liu, M., Gao, Y., Wang, W., Shi, Y., An, M., Zhang, Y., Liu, X., 2017. Lithospheric structure across the northeastern margin of the Tibetan Plateau: Implications for the plateau's lateral growth. Earth Planet. Sci. Lett. 459, 80–92, doi: 10.1016/j.epsl.2016.11.027.

Shen, Z., Wang, M., Li, Y., Jackson, D.D., Yin, A., Dong, D., Fang, P., 2001. Crustal deformation along the Altyn Tagh fault system, western China, from GPS. J. Geophys. Res. 106, 607–621, doi: 10.1029/2001JB000349.

Shi, L., Li, Y., Wang, W., Ma, Y., 2022. Crustal structure beneath the northeastern margin of the Tibetan Plateau constrained by receiver functions and gravity data. Tectonophysics 841, 229584, doi: 10.1016/j.tecto.2022.229584.

Sundell, K.E., Taylor, M.H., Styron, R.H., Stockli, D.F., Kapp, P., Hager, C., Liu, D., Ding, L., 2013. Evidence for constriction and Pliocene acceleration of east-west extension in the North Lunggar rift region of west central Tibet. Tectonics 32, 1454–1479, doi: 10.1002/tect.20086.

Tapponnier, P., Mercier, J.L., Armijo, R., Tonglin, H., Ji, Z., 1981. Field evidence for active normal faulting in Tibet. Nature 294, 410–414, doi: 10.1038/294410a0.

Trifonov, V.G., Zelenin, E.A., Sokolov, S.Yu., Bachmanov, D.M., 2021. Active tectonics of Central Asia. Geotectonics 55, 361–376, doi: 10.1134/S0016852121030092.

Wang, E., Kirby, E., Furlong, K.P., Van Soest, M., Xu, G., Shi, X., Kamp, P.J.J., Hodges, K.V., 2012. Two-phase growth of high topography in eastern Tibet during the Cenozoic. Nat. Geosci. 5, 640–645, doi: 10.1038/ngeo1538.

Wang, M., Shen, Z.K., 2020. Present-day crustal deformation of continental China derived from GPS and its tectonic implications. J. Geophys. Res. Solid Earth 125, e2019JB018774, doi: 10.1029/2019JB018774.

Wang, M., Shen, Z., Niu, Z., Zhang, Z., Sun, H., Gan, W., Wang, Q., Ren, Q., 2003. Contemporary crustal deformation of the Chinese continent and tectonic block model [in Chinese]. Sci. China (Ser. D), 33 (z1), 21–33, doi: 10.1360/03dz0003.

Wang, Q., Zhang, P., Freymueller, J.T., Bilham, R., Larson, K., Lai, X., You, X., Niu, Z., Wu, J., Li, Y., Liu, J., Yang, Z., Chen, Q., 2001. Present-day crustal deformation in China constrained by global positioning system measurements. Science 294, 574–577, doi: 10.1126/science.1063647.

Wang, W., Zheng, W., Zhang, P., Li, Q., Kirby, E., Yuan, D., Zheng, D., Liu, C., Wang, Z., Zhang, H., Pang, J., 2017. Expansion of the Ti-

betan Plateau during the Neogene. Nat. Commun. 8, 15887, doi: 10.1038/ncomms15887.

Wei, W., Unsworth, M., Jones, A., Booker, J., Tan, H., Nelson, D., Chen, L., Li, S., Solon, K., Bedrosian, P., Jin, S., Deng, M., Ledo, J., Kay, D., Roberts, B., 2001. Detection of widespread fluids in the Tibetan crust by magnetotelluric studies. Science 292, 716–719, doi: 10.1126/science.1010580.

Wessel, P., Luis, J.F., Uieda, L., Scharroo, R., Wobbe, F., Smith, W.H.F., Tian, D., 2019. The generic mapping tools Version 6. Geochem. Geophys. Geosyst. 20, 5556–5564, doi: 10.1029/2019GC008515.

Woodruff, W.H., Jr., Horton, B.K., Kapp, P., Stockli, D.F., 2013. Late Cenozoic evolution of the Lunggar extensional basin, Tibet: Implications for basin growth and exhumation in hinterland plateaus. GSA Bull. 125, 343–358, doi: 10.1130/B30664.1.

Wu, X., Xiang, Y., Tang, F., 2020. Study on current crustal deformation of the Himalayan tectonic zone by GPS strain-rate estimation and focal mechanism stress inversion [in Chinese]. Chin. J. Geophys. 63, 2924–2939, doi: 10.6038/cjg2020N0362.

Xia, S., Shi, L., Li, Y., Guo, L., 2021. Velocity structures of the crust and uppermost mantle beneath the northeastern margin of Tibetan plateau revealed by double-difference tomography [in Chinese]. Chin. J. Geophys. 64, 3194–3206, doi: 10.6038/cjg2021O0514.

Xu, Q., Hetzel, R., Hampel, A., Wolff, R., 2021. Slip rate of the Danghe Nan Shan thrust fault from ^{10}Be exposure dating of folded river terraces: implications for the strain distribution in Northern Tibet. Tectonics 40, e2020TC006584, doi: 10.1029/2020TC006584.

Xu, X., Wang, F., Zheng, R., Chen, W., Ma, W., Yu, G., Chen, G., Tapponnier, P., van der Woerd, J., Meriaux, A.S., Ryerson, F.J., 2005. Late Quaternary sinistral slip rate along the Altyn Tagh fault and its structural transformation model. Sci. China Ser. D: Earth Sci. 48, 384–397, doi: 10.1360/02yd0436.

Yang, H., Yang, X., Zhang, H., Huang, X., Huang, W., Zhang, N., 2018. Active fold deformation and crustal shortening rates of the Qilian Shan Foreland Thrust Belt, NE Tibet, since the Late Pleistocene. Tectonophysics 742–743, 84–100, doi: 10.1016/j.tecto.2018.05.019.

Yang, H., Wang, D., Guo, R., Xie, M., Zang, Y., Wang, Y., Yao, Q., Cheng, C., An, Y., Zhang, Y., 2022. Rapid report of the 8 January 2022 M_s 6.9 Menyuan earthquake, Qinghai, China. Earthquake Res. Adv. 2, 100113, doi: 10.1016/j.eqrea.2022.100113.

Yang, Z., Chen, Y., Zhang, X., Song, X., 2019. S-wave velocity structure and radial anisotropy in eastern and north-eastern margins of Tibetan plateau [in Chinese]. Chin. J. Geophys. 62, 4554–4570, doi: 10.6038/cjg2019N0149.

Yao, H., Beghein, C., van der Hilst, R.D., 2008. Surface wave array tomography in SE Tibet from ambient seismic noise and two-station analysis – II. Crustal and upper-mantle structure. Geophys. J. Int. 173, 205–219, doi: 10.1111/j.1365-246X.2007.03696.x.

Yao, W., Liu-Zeng, J., Oskin, M.E., Wang, W., Li, Z., Prush, V., Zhang, J., Shao, Y., Yuan, Z., Klinger, Y., 2019. Reevaluation of the Late Pleistocene slip rate of the Haiyuan fault near Songshan, Gansu Province, China. J. Geophys. Res. Solid Earth 124, 5217–5240, doi: 10.1029/2018JB016907.

Yin, A., Harrison, T.M., 2000. Geologic evolution of the Himalayan-Tibetan orogen. Annu. Rev. Earth Planet. Sci. 28, 211–280, doi: 10.1146/ANNUREV.EARTH.28.1.211.

Yuan, D.Y., Champagnac, J.D., Ge, W.P., Molnar, P., Zhang, Z.P., Zheng, W.J., Zhang, H.P., Liu, X.W., 2011. Late Quaternary right-lateral slip rates of faults adjacent to the lake Qinghai, northeastern margin of the Tibetan Plateau. GSA Bull. 123, 2016–2030, doi: 10.1130/B30315.1.

Zhang, B., Zheng, W., Li, T., Wang, W., Chen, J., Li, Z., Li, X., Duan, L., 2022. Late Cenozoic fold deformation in the northern margin of Qaidam Basin and southward propagation of Qilian Shan. Tectonophysics 822, 229153, doi: 10.1016/j.tecto.2021.229153.

Zhang, P.-Z., Shen, Z., Wang, M., Gan, W., Bürgmann, R., Molnar, P., Wang, Q., Niu, Z., Sun, J., Wu, J., Hanrong, S., Xinzhao, Y., 2004. Continuous deformation of the Tibetan Plateau from global positioning system data. Geology 32, 809–812, doi: 10.1130/G20554.1.

Zhang, P.-Z., Molnar, P., Xu, X., 2007. Late Quaternary and present-day rates of slip along the Altyn Tagh Fault, northern margin of the Tibetan Plateau. Tectonics 26, TC5010, doi: 10.1029/2006TC002014.

Zheng, D., Wang, W., Wan, J., Yuan, D., Liu, C., Zheng, W., Zhang, H., Pang, J., Zhang, P., 2017a. Progressive northward growth of the northern Qilian Shan–Hexi Corridor (northeastern Tibet) during the Cenozoic. Lithosphere 9 (3), 408–416, doi: 10.1130/L587.1.

Zheng, G., Wang, H., Wright, T.J., Lou, Y., Zhang, R., Zhang, W., Shi, C., Huang, J., Wei, N., 2017b. Crustal deformation in the India-Eurasia collision zone from 25 years of GPS measurements. J. Geophys. Res. Solid Earth 122, 9290–9312, doi: 10.1002/2017JB014465.

Zheng, W.-j., Zhang, P.-z., He, W.-g., Yuan, D.-y., Shao, Y.-x., Zheng, D.-w., Ge, W.-p., Min, W., 2013. Transformation of displacement between strike-slip and crustal shortening in the northern margin of the Tibetan Plateau: Evidence from decadal GPS measurements and late Quaternary slip rates on faults. Tectonophysics 584, 267–280, doi: 10.1016/j.tecto.2012.01.006.